EUROPEAN FUSION DEVELOPMENT AGREEMENT

EFDA–JET–PR(03)01

V.Yavorskij, V.Goloborodko, K.Schoepf, S.Sharapov,
C.D. Challis, S.Reznik, D. Stork

Confinement of Fusion Alpha-Particles in JET Hollow Current Equilibrium

Confinement of Fusion Alpha-Particles in JET Hollow Current Equilibrium

V.Yavorskij[1, 2], V.Goloborodko[1, 2], K.Schoepf[1],
S.Sharapov[3], C.D. Challis[3], S.Reznik[1, 2], D. Stork[3]

[1]*Institute for Theoretical Physics, University of Innsbruck, Austria, Association EURATOM-OEAW*
[2]*Institute for Nuclear Research, Kiev, Ukraine*
[3]*Euratom/UKAEA Fusion Association, Culham Science Centre, Abingdon, Oxfordshire OX14 3DB, UK*

Preprint of Paper to be submitted for publication in
Nuclear Fusion

ABSTRACT.
The effect of a toroidal current hole on the first orbit loss and on the collisional loss of alpha particles in JET is investigated. Numerical results of predictive 3D Fokker-Planck modelling of the distribution function of D-T fusion alphas in hollow current JET discharges are presented. If the current hole region is kept reasonably small, it induces only a moderate increase of first orbit losses as well as of the collisional loss of fast alphas. The current hole effect is shown to be qualitatively equivalent to a reduction of the total plasma current I. Hence the alpha confinement degradation by hollow current profiles can be compensated by enlarging I.

1. INTRODUCTION

Recent tokamak experiments [1–4] have successfully demonstrated operational scenarios with Internal Transport Barriers (ITBs), which provide improved plasma core energy confinement at reduced inductive current. Hollow current profiles typical for these scenarios can lead to plasma equilibrium states that are stable over remarkably long periods. A hollow profile of the toroidal plasma current, i.e. the current profile with zero current density at the plasma centre (the current hole), allows the generation of the ITBs delivering high fusion performance at small input power. Thus, such configurations could be regarded as serious candidates for stationary operation of a fusion tokamak-reactor with a strong bootstrap current fraction. Although the scenario for a stationary tokamak has been long searched for, e.g. Refs. [5–8], the experimental evidence for scenarios of such type was obtained only recently, when the regimes with ITBs had become technically feasible [9–11]. While the confinement of the bulk plasma is extremely good in the ITB scenario, the confinement of 3.5 MeV fusion-born α-particles remains to be thoroughly investigated in order to assess the envisaged reactor operation regime.

In this paper we examine the effect of the toroidal current hole on the first orbit (FO) loss and on the collisional loss of α's [12, 13], due to the pitch-angle scattering of marginally circulating counter-going alphas into unconfined fat bananas, and due to neoclassical (NC) radial transport. We present also a predictive modelling of the distribution function of D-T fusion alphas in hollow current JET discharges. The relevant profiles of current density, safety factor, fusion product source term, ion and electron densities and temperatures are taken in accordance with actual reference profiles measured in JET deuterium discharges.

We note that the predictive modelling of alpha particle confinement in JET is of essential interest in view of the development of the energetic ion loss diagnostics for JET [14].

The paper is organised in the following way. In Section 2 the model of JET magnetic configurations associated with hollow current profiles is elaborated and an analysis of corresponding single ion orbits is performed. The effect of the current hole on the FO loss fraction of 3.5 MeV alphas and on the alpha loss distributions over poloidal and pitch-angles is investigated in Section 3. In Section 4 the results of 3D Fokker-Planck calculations of collisional alpha loss in JET hollow current configurations are presented. Section 5 is devoted to the distribution function of confined alphas,

wherefrom their power deposition into electrons and ions is calculated as well as the alpha driven bootstrap current contribution. The results are summarized and discussed in Section 6.

2. SINGLE ION ORBITS IN JET HOLLOW CURRENT EQUILIBRIUM STATES

Our investigation is based on a semi-analytical model for magnetic field [15] with the hollow current profiles and flux surface shape obtained via Motional Stark Effect (MSE) measurements [2] for a specific JET reference discharge (pulse #51976). Figure 1 displays the reference hollow current density profile measured in JET shot #51976 at t = 44.8 s. This profile is well approximated by

$$j \propto \left[1 - (1 - \phi^{1/2})^{l}\right]^{mn} (1 - \phi)^{n} \qquad (1)$$

where $\phi = \Phi(r)/\Phi(a) \equiv x^2$ denotes the normalized toroidal flux, r the flux surface radius, a the minor plasma radius, $m = 2[(1 - \phi_m^{1/2})^{-2} - 1]/(1 + \phi_m^{-1/2})/l$, and $\phi_m^{1/2} = x_{\rm m}$ determines the radial position of the maximum toroidal current density and l, n are positive numbers. The best approximation for the current density profile $j(\phi)$ is obtained with $l = 6$ and $n = 2$, which reasonably approximates the measured hollow current density shape both in JET ($x_{\rm m} = 0.45$, shot #51976) and in JT-60 ($x_{\rm m} = 0.6$, see [3, 4]). To reconstruct the q-profiles for hollow JET currents we suppose the following profiles for the flux surface (FS) parameters: (i) Shafranov shift $\Delta(r) = \Delta_0[1 - (r/a)^2]$, (ii) elongation $k(r) = k_a - [k_a - k_0][1 - (r/a)^2]^2 - 0.5k_a'(r/a)^2[1 - (r/a)^2]$, (iii) triangularity $\Lambda(r) = \Lambda_a(r/a)^2$, with the boundary values at $r = 0$ and $r = a$ taken similar to the ones measured in the reference shot #51976: $\Delta_0 = 0.15$ m, $k_a = 1.7$, $k_0 = 0.9$, $\Lambda_a = 0.28$. The only undefined value k_a' is chosen from the condition that the modelled and the measured safety factor $q(a)$ coincide at the plasma edge, yielding $k_a' \sim 0.8$. The reconstructed profiles determining the hollow current JET magnetic configuration are shown in Figures 2 and 3. As can be seen, our reconstructed q-profiles are in satisfactory agreement with the MSE profile. Note that normalized flux surface radius, r/a, can be easily determined as a function of the radial coordinate $x \equiv \phi^{1/2}$ (square root of the normalized toroidal flux, see Figure 3) from the simple relation $x = r/a(0.63 + 0.37r/a)$ with an accuracy of 1%.

It should be mentioned that, in the case of rather small current hole, $x_{\rm m} \sim 0.3$, the safety factor profile qualitatively is similar to an inverse rotational transform of a stellarator. Indeed, for $x_{\rm m} = 0.34$ the power index $m(x_{\rm m}, l = 6) = 1$, and the rotational transform, q^{-1}, in the hollow current area behaves like the paraxial rotational transform in a stellarator with multipolarity 3, i.e. $q^{-1} \sim x^2$.

We note first that in tokamak hollow current configurations exhibiting equal total toroidal current and flux surface geometry, the size of the current hole strongly affects the q-profile in the central part of plasma, $x < x_{mq}$ (here $x_{mq} \approx x_{\rm m}$ is the radial position of the minimum q-value), while the effect of the current hole extent on $q(x)$ in the plasma periphery, $x > x_{mq}$, is less significant (see Figure 2). Examining the fast particle orbits in hollow current profiles, one expects therefore that only particles moving through the core plasma, $x < x_{mq}$, feel the current hole. This is confirmed by Figure 4a, which demonstrates how a change of the current hole radius relocates the 3.5 MeV alpha gyro-orbit in I/B = (2 MA)/(3.45 T) JET hollow current discharges with fixed flux surfaces. The

particle starts at $R_0 = 3.2$ m on the plasma equatorial plane ($Z = 0.33$ m), corresponding to an initial flux surface radius $r_0/a = 0.15$ ($x_0 \approx 0.11$). In a cylindrical coordinate system (R, Z, φ), the initial velocities of the considered particle are $V_{R0} = V_{Z0} = 0.698V$. Comparing the cases $x_m = 0.3$ and $x_m = 0.45$, when the particle is well confined or, respectively, marginally confined, with an extended current hole scenario such that the maximum of the plasma current density appears at $x_m = 0.6$, the banana width is drastically enlarged resulting in the escape of the particle well below the mid-plane. Figure 4b demonstrates the same effect for a 1 MeV alpha particle that starts at $R_0 = 3.33$ m on the equatorial plane ($r_0/a = 0.3$, $x_0 \approx 0.22$) with initial velocity components $V_{R0} = V_{Z0} = 0.587V$. This effect is even stronger for orbits passing the central plasma region. For a 3.5 MeV and a 0.35 MeV alpha both passing through $r = 0$, we present in Figure 5 the maximum radial coordinate, r_{GCmax}, reached by their respective guiding centre orbit, as a function of the pitch angle cosine $\xi = V_{||}/V$ at $r = 0$ for a monotonic current profile and two hollow current profiles. It is seen that the current hole results in the loss of a significant fraction (up to 10% at $x_m = 0.6$) of 3.5 MeV paraxial alphas (marginally trapped ones); all of them were confined in the case of monotonic $j(r)$. For simplicity we suppose here that a trapped particle is lost if its guiding centre reaches the plasma edge, which is correct if the particle gyro radius is comparable to the gap between the outmost closed FS and first wall. By inspection of Figure 4 this supposition looks reasonable at least for MeV alphas in the magnetic configurations considered here. However, if the gap reduces to 0, the effect of finite gyro radius for FO loss may become important, because the maximum radial coordinate of the particle orbit exceeds that of the guiding centre orbit (compare full and dashed lines in Figure 5), and thus results in additional loss of at least a few percent of fusion alphas. The most significant enlargement of the particle orbit width, Δr, takes place for low–energy particles (with $\Delta r << a$ in the case of monotonic current), first of all for circulating ones, passing the paraxial area $x < x_{mq}$.

According to simple orbit analysis applied to the case $q^{-1} \sim j \sim x^{2m}$, the radial excursions of the guiding centre of circulating particles due to the toroidal drift are given by

$$\Delta r_u \propto R\Delta^{1/(1+2m)},\ \Delta = \frac{2q_a\rho_L}{Rk_a} = \frac{I_*}{IA}\ \frac{k_a + k_a^{-1}}{2}\ F(A, k_a, \Lambda_a), \qquad (2)$$

where $I_* = m_\alpha c^2 V_\alpha/(2e_\alpha)$, m_α and e_α are respectively the particle mass and the charge, $I_*(E_\alpha = 3.5MeV) = 1.35MA$, factor $F(A, k_a, \Lambda_a) \sim 1$ describes the effect of FS non-circularity [15]. Analogously, for trapped particles ($-\Delta^{1/(3+4m)} < \xi < 0$) crossing the paraxial area we obtain the estimate of the orbit width as

$$\Delta r_t \propto R\Delta^{2/(3+4m)} \qquad (3)$$

In the particular case of $m = 0$ and $m = 1$ these expressions coincide with those obtained correspondingly for tokamak with monotonic current [16] and for a stellarator with multipolarity 3 [17]. From the above and from $m(x_m, l = 6) = [(1 - x_m)^{-6} - 1]/(1 + 1/x_m)/3$ it follows that the energy dependence of the radial excursions of particles passing the current hole area weakens drastically

with increasing x_m. Thus for $x_m = 0.45$ ($m = 3.6$) we have $\Delta r_t \sim E^{0.057}$ and $\Delta r_u \sim E^{0.060}$. It is important to note that the ratio of paraxial excursions of trapped and circulating particles, $\Delta r_t/\Delta r_u \sim \Delta^{1/[(3+4m)(1+2m)]}$ becomes almost independent of energy and is of the order of unity for $x_m > 0.3$–0.4 not only for the ions in the MeV range of energy, but even for thermalized ions.

Inspecting the confinement domains [12] in the plane spanned by the normalized magnetic moment $\lambda = \mu B_0/E$ and the normalized radial coordinate r_{max}/a, where r_{max} is the maximum guiding centre radial coordinate along the bounce orbit, Figure 6 demonstrates a substantial reduction of the confinement domain for alphas at birth energy $E_0 = 3.5$ MeV as the current hole region is enlarged (increasing x_m). The solid curves in this figure represent the maximum value of λ for co- ($V_{||}/V>0$ at $r = r_{max}$) and counter- ($V_{||}/V<0$ at $r = r_{max}$) going particles that correspond to stagnation co- and counter-going orbits, respectively. The dotted lines indicate the trapped/passing separatrix in the $\{\lambda, r_{max}\}$ plane, while for counter-circulating orbits they also represent a part of the confinement domain boundary. The dashed line gives the part of the confinement domain boundary of counter-circulating particles at rather low λ, for which r_{max} of the corresponding fattest bananas is greater than a. Therefore counter-circulating particles can scatter through this part of the boundary into lost fat banana orbits. Consequently it is called cone loss boundary.

Evidently a confinement domain reduction would result in the essential enhancement of the collisional loss of alpha particles. The next important effect of the current hole is the absence of confined fattest bananas in the MeV energy range (absence of the separatrix between co- and counter-moving particles in the confinement domain in Figure 6b), which makes the collisional exchange between trapped and circulating alphas through the trapped/passing boundary impossible.

3. FIRST ORBIT LOSS OF FUSION ALPHAS

To calculate the FO and collisional loss of fusion alphas, two shapes of the alpha source term were used,

$$S_1 \propto \exp(-33\phi^{3/2}) + 30.7\phi^2\exp(-11\phi) \text{ and } S_2 \alpha\, n_d n_t \langle\sigma V\rangle, \qquad (4)$$

where n_d and n_t denote the deuteron and triton density, respectively, and $\langle\sigma V\rangle$ the fusion reaction rate. Using $p(x) = 1 - ((x - x_m^*)/(1 - x_m^*))^2 \Theta(x - x_m^*)$ with $\Theta(x)$ denoting the Heaviside step function, and choosing $x_m^* = 0.45$, the plasma parameters taken were $T_e = 10\,p(x)$ keV, $T_d = T_t = 20p(x)$ keV, $n_e = 0.5 \times 10^{20}\,p(x)\,m^{-3}$, $n_d = n_t$, and $Z_{eff}(x) = 1.5 + 2.4x^2/(1 + 4x^{20})$ caused by CVI carbon impurity. Figure 7 displays the fusion source profiles given by Equation (4) in comparison with the TRANSP profiles of the DD neutrons for the reference deuterium plasma shot #51976 for times 44.8 s, 45.3 s and 45.8 s. The source terms, S, in this figure are normalized to their volume-averaged values, $\langle S\rangle \equiv \int dr S/\int dr$. It can be seen that a Gaussian-like profile S_1 for alpha-particles in a DT plasma satisfactory approximates the normalized profiles of JET DD neutron rates in the reference shot #51976 during the time interval 44.8 s $\le t \le$ 45.8 s. Note that the chosen non-monotonic profile $Z_{eff}(x)$, with a maximum $Z_{eff} \approx 3$ at $x \approx 0.85$ and $Z_{eff}(a) \ge 2$ is in a satisfactory quantitative agreement

with that measured in shot #51976 (t = 44.9s).

The FO loss fractions of fusion alphas, L_{FO}, calculated as a function of the maximum current density position are displayed in Figure 8 for plasma currents $2MA \le I \le 3MA$. An increase of the current hole size according to the shift of x_m from 0.1–0.2 to 0.6 results, in the case of a rather steep JET fusion source profile ($S(r) = S_1(r)$), in the enhancement of alpha loss from 7% to 23% for a plasma current I = 3 MA and, respectively, from 20% to 40% for I = 2 MA. It is important that at $S(r) = S_1(r)$ the effect of current hole becomes significant only at rather high values of $x_m >$ (0.3–0.4). FO losses of alphas in DT operation with a moderately flat fusion source profile ($S(r) = S_2(r)$) appear about 1.5 times enlarged when compared to $S(r) = S_1(r)$ and are sensitive even to the small size current hole. Transition from a monotonic to a strongly hollow current with x_m = 0.6 enhances the FO alpha loss more then 2 times, up to (35–55)% at $2MA \le I \le 3MA$. A significant here is the following observation, at rather high x_m (>0.3–0.4), the effect of the current hole on alpha loss is equivalent to the effect of the decrease of the total plasma current. It can be seen from Figure 8 that a shift of the current density maximum position from x_m = 0.45 to x_m = 0.6 corresponds to the effect of a total current decrease of about 0.5 MA.

Important from the point of view of the first wall load as well as of the envisaged alpha loss JET diagnostics [14] is the FO alpha loss flux distribution $\Gamma(\zeta, \theta)$ over the pitch angle ζ and the poloidal angle θ, i.e. $\Gamma(\zeta, \theta)d\zeta d\theta$ gives the number of particles that hit the first wall per m^2 and s at polidal angles within the interval $[\theta, \theta + d\theta]$, and had, at the moment of impingement, a direction of motion within the interval $[\zeta, \zeta + d\zeta]$. Figure 9 displays the variation of this distribution with increasing size of the current hole for $I = 2.5MA$ and for the steep $S(r) = S_1(r)$ alpha source term. The poloidal angle θ here is the angle measured from the plasma midplane $Z = Z_{ax} = 0.33m$ of the polar coordinate system with its centre at R = 2.9 m, and the pitch angle is determined as $\zeta = cos^{-1}(V_{||}/V)$ at $r = a$. Poloidal angles $90^o \le \theta \le 106^o$ correspond to the divertor area. Due to the strong sharp dependence of the maximum radial coordinate on the longitudinal energy (see Figure 5) near the trapped/circulating boundary the FO loss are strongly localized in pitch angle. The maximum loss takes place at pitch angles $\zeta = \zeta_s + (5^o \div 10^o)$ and poloidal angles $55^o \div 60^o \le \theta \le 100^o \div 105^o$, where $\zeta_s = \zeta_s(\theta)$ corresponds to the lost fattest bananas and varies from $\zeta_s(\theta = 0^o) \approx 55^o \div 60^o$ to $\zeta_s(\theta = 180^o) > 90^o$ as shown by the shadowed line in Figure 9. The transition from monotonic to hollow current profiles with x_m = 0.6 enlarges the maximum FO loss about 2.5 times and shifts this maximum from poloidal angles $\theta \approx 55^o \div 60^o$ below the midplane to rather high angles $\theta \ge 100^o \div 105^o$ corresponding to the divertor area. At fixed hollow current profile with x_m = 0.45 the effect of increasing (decreasing) I (see Figures 10a, b) is very similar to the decrease (increase) of the current hole size at fixed plasma current (see corresponding Figures 9a, c). Operation with a flat fusion source term results in the pitch-angle broadening of the alpha loss as shown in Figure 10c.

It is important that the poloidal distribution of the total FO loss flux $\Gamma(\theta) = \int d\zeta sin\zeta\, \Gamma(\zeta, \theta)$ (see Figure 11) is rather broad with typical peaking factors $p = \Gamma_{max}/\langle\Gamma\rangle$ (the ratio of maximum alpha loss flux to the flux of lost alphas averaged over the first wall) of order 3.5 ÷ 4. Consequently, for

$I \geq 2.5$ MA and x_m<0.5 where $L_{FO} \leq 0.3$, the maximum alpha heat load is $W_\alpha \sim 0.25 p W_n \times L_{FO} \sim (0.25 \div 0.3) W_n$, where W_n is the neutron heat load. We note, however, that our consideration is based on the supposition of a smooth first wall. In the presence of uneven first wall areas (due to structures such as divertor, and antennas) the poloidal distribution of alpha loss may essentially deviate from that obtained here. Finally, Figure 12 represents the pitch-angle distributions of lost alphas at the poloidal angle $\theta = 40^o$ which is close to the position of the envisaged alpha loss measurements [14]. It is important that FO losses are strongly localised in the vicinity of pitch-angles of lost fattest bananas $\zeta \approx 60^o$ featuring a typical half-width $\Delta\zeta \approx 6^o$–10^o in the case of peaked source term. However for the flat source profile $S = S_2$, the pitch-angle distribution of prompt alpha loss is substantially broader with a half-width of FO loss $\Delta\zeta \approx 15^o$.

4. COLLISIONAL LOSS OF FUSION ALPHAS

Our kinetic calculations of charged fusion product losses are based on a 3D (in the constants-of-motion space) steady state Fokker-Planck code [12, 13]. The transport coefficients of the present Fokker-Planck modelling include only axisymmetric contributions resulting from the slowing down of alphas as well as from their pitch-angle scattering on the bulk plasma particles. It should be pointed out that a weak rotational transform in the central area of the JET hollow current configuration essentially enhances the rate of neoclassical diffusion of alphas ($\sim D_{rr}/(\Delta r)^2$), not only because of the increment of their radial diffusion coefficient $D_{rr} \sim D_{\lambda\lambda} (\partial r_{\max}/\partial\lambda)^2 \sim \nu_\perp (\Delta r_t)^2/(\Delta\lambda_t)^2$ (the subscript (t) indicates toroidally trapped particles) but also due to the decrease of the radial size of the confinement domain of these particles, $\Delta r \leq a - r_{\min}(\lambda = 0)$; in the preceding expressions $D_{\lambda\lambda} \sim \nu_\perp$ denotes the pitch-angle scattering diffusion coefficient and $r_{\min}(\lambda = 0)$ is the FS radius of the 'best confined' stagnation orbits with $V_\parallel = \pm V$. Note that, contrary to conventional monotonic profiles $j(r)$ where $r_{\min}(\lambda = 0)/a \sim q(0)\rho_L/a << 1$, we have in the presence of current hole $r_{\min}(\lambda = 0)/a \sim (q(a)\rho_L/a)^{1/(1+2m)}$ measuring up to ~ 0.3–0.4. Thus, in the case $x_m = 0.45$, $r_{\min}(\lambda = 0, \sigma = -1)$ is about $0.33a$ for 3.5 MeV counter-going alphas, and the corresponding reduction of the confinement domain in the radial coordinate is more than 30%. For the I/B = 2.5 MA/3.45 T JET hollow current equilibrium with $x_m = 0.45$, Figure 13 displays the contours of the bounce-averaged pitch-angle scattering diffusion coefficient, $D_{\lambda\lambda}$ (Figures 13*a*, 13*b*), and further the contours of the bounce-averaged radial diffusion coefficient, D_{rr} (Figures 13*c*, 13*d*), of $3.5MeV$ co-going (Figures 13*a*, 13*c*) and counter-going (Figures 13*b*, 13*d*) alphas in the $\{\lambda, r_{max}\}$-plane. In this figure $D_{\lambda\lambda}$ is normalized to its maximum value, ~ 0.02 s^{-1}, that eventuates for co-circulating particles with $\lambda = 0.5$ and $r_{max} = 0.7a$, while the radial diffusion coefficient D_{rr} is normalized to the value $[a - r_{\min}(\lambda = 0, \sigma)]^2 \times \max\{D_{\lambda\lambda}\}$. Whereas the pitch-angle scattering is most effective for circulating particles with $0.2 < \lambda < 0.8$, the neoclassical radial diffusion is seen to be most important for trapped alphas with $\lambda \sim 1$ as well as for a small fraction of marginally circulating counter going alphas. For the latter (due to their strong sensitivity to pitch angle scattering, $\partial r_{max}/\partial\xi \to \infty$) the neoclassical radial diffusion reaches even the extremely high banana plateau level ($\sim (\Delta r_b)^2 \omega_b$), which is a few orders of magnitude higher than D_{rr} for the rest of the particles

[18]. However this high banana plateau level of radial diffusion is associated with only a very small number of counter-circulating particles. It is important to note that the rate of radial diffusion exceeds the pitch-angle scattering rate for both trapped and counter-circulating particles. Therefore neoclassical transport essentially affects the distribution function of alphas, $f_\alpha(r,V)$, contrary to the bulk plasma particles, of which the distribution function $f_{i,e}(r,V)$ is shaped dominantly by the transport in velocity space and only weakly influenced by neoclassical transport. Nevertheless the rates of pitch-angle scattering and radial transport of fusion alphas are small as compared to the slowing down rate, ν_s ($\max\{\nu_s\} \cong 70 \cdot \max\{D_{\lambda\lambda}\}$ for co-going 3.5*MeV* alphas). Thus for MeV-alphas and the plasma parameters considered, we have typically the relationship $D_{\lambda\lambda}/(\Delta\lambda)^2 < D_{rr}/(\Delta r)^2 \sim 10^{-2}\nu_s$. It should be pointed out that, despite the smallness of the ratios of neoclassical diffusion and, respectively, pitch-angle rates to the slowing down collisional rate, ν_s, the fraction of collisionally lost alphas is not unimportant and cannot be neglected for the majority of fusion alphas [19]. The reason of the enhanced collisional loss ($>> \nu_\perp/\nu_s \sim 10^{-2}$) is the rather steep slope in the dependence of the initial distribution function of confined alphas on the coordinates $c \equiv \{c_1, c_2\} = \{\lambda, r_{max}\}$, i.e. $|\partial lnf_\alpha/\partial lnc_i| >> 1$, resulting in collisional loss fractions of fast alphas $L_{coll} \sim (D_{\lambda\lambda}/\nu_s)^{1/2} \sim (D_{rr}/[a - r_{min}(\lambda = 0, \sigma)]^2\nu_s)^{1/2} \sim 0.1$ essentially exceeding the ratio $\nu_\perp/\nu_s \sim 10^{-2}$. This is confirmed by Figure 14 where we display the calculated loss fractions L_{NC} and L_{cone} of alphas in the energy range $0.0625 < E/E_0 < 1$ as caused by their radial neoclassical diffusion and scattering into the loss cone through the passing/trapped boundary, respectively; further shown is the total collisional loss as a function of the radial position of the hollow current density maximum.

In the case of a steep fusion source profile the dependence of the collisional loss on x_m is similar to that of the FO loss, i.e. it depends only weakly on the current profile if $x_m < 0.4$–0.5, while a substantial current hole loss enhancement is observed at rather high x_m (> 0.4–0.5). Interestingly, if $x_m < 0.3$, the collisional loss even decreases with x_m in the case of a flat $S = S_2$ fusion profile; obviously, this is due to the reduced number of confined alphas ($\sim 1 - L_{FO}$) as a result of the enlarged FO loss. Also note that for the case 2 MA < *I* < 3 MA and $x_m < 0.6$ considered here the alpha loss fraction due to radial diffusion, $L_{NC} \approx (3$–$6)\%$, is comparable to the cone loss fraction, $L_{cone} \approx (3$–$9)\%$. Further we list in Tables 1, 2 and 3 for the cases of JET-like fusion source terms and *I/B* = (2, 2.5, 3 MA)/(3.45 T) the collisional and FO alpha loss fractions, respectively, for a monotonic toroidal current scenario and for hollow current density profiles exhibiting $x_m = 0.45(0.6)$.

Table 1: First orbit and collisional loss fractions of fusion alphas in JET hollow current equilibrium with $x_m = 0.45$ for a fusion source term $S = S_1$ (shot #51976). Loss fractions are in percents, collisonal losses take into account lost alphas with energies $E > 0.0625\ E_0 = 220$ keV. The superscripts on NC indicate toroidally trapped (t), co-circulating (+) and counter-circulating (-) particles.

I		*Collisional particle loss fractions* L					*Collisional energy loss fractions*				
[MA]	*FO*	*cone*	NC^t	NC^+	NC^-	*total*	*cone*	NC^t	NC^+	NC^-	*total*
2	28.4	6.8	4.2	0.27	0.26	11.5	3.6	1.9	0.25	0.18	6.0
2.5	19.6	5.4	3.1	0.26	0.20	8.9	3.4	1.8	0.24	0.15	5.6
3	12.3	3.7	2.2	0.16	0.19	6.2	2.4	1.4	0.15	0.15	4.1

Table 2: First orbit and collisional loss fractions of fusion alphas in JET hollow current equilibrium with x_m = 0.6 for the fusion source term S = S_1 (shot #51976). Loss fractions are in percents, collisonal losses take into account lost alphas with energies $E > 0.0625\ E_0$ = 220 keV.

I		*Collisional particle loss fractions* L					*Collisional energy loss fractions*				
[MA]	*FO*	*cone*	NC^t	NC^+	NC^-	*total*	*cone*	NC^t	NC^+	NC^-	*total*
2	40.3	9.4	5.0	0.22	0.40	15.0	3.4	2.0	0.20	0.29	5.9
2.5	30.0	7.8	4.0	0.16	0.18	12.2	3.8	1.9	0.15	0.13	6.0
3	22.4	5.8	2.8	0.13	0.11	8.8	3.5	1.6	0.12	0.09	5.3

Table 3: First orbit and collisional loss fractions of fusion alphas for a monotonic current profile in JET and for the fusion source term S = S_1 (shot #51976). Loss fractions are in percents, collisonal losses take into account lost alphas with energies $E > 0.0625\ E_0$ = 220 keV.

I		*Collisional particle loss fractions* L					*Collisional energy loss fractions*				
[MA]	*FO*	*cone*	NC^t	NC^+	NC^-	*total*	*cone*	NC^t	NC^+	NC^-	*total*
2	20.8	5.8	3.6	0.38	0.35	10.1	3.3	1.7	0.36	0.25	5.7
2.5	12.4	3.7	2.9	0.73	0.28	7.6	2.2	1.9	0.69	0.21	5.0
3	7.8	2.7	2.3	0.72	0.25	5.9	1.6	1.8	0.68	0.20	4.3

Table 4: First orbit and collisional loss fractions of fusion alphas in monotonic and hollow current equilibria with *I/B* = (2.5 MA)/(3.45 T) and for the flat fusion source term S = S_2. Loss fractions are in percents, collisonal losses account for lost alphas with energies $E > 0.0625\ E_0$ = 220 keV.

		Collisional particle loss fractions L					*Collisional energy loss fractions*				
x_m	*FO*	*cone*	NC^t	NC^+	NC^-	*total*	*cone*	NC^t	NC^+	NC^-	*total*
0	17.9	4.9	3.1	1.1	0.39	9.4	2.7	2.0	1.0	0.30	6.0
0.45	31.0	5.7	2.9	0.38	0.29	9.2	3.2	1.6	0.36	0.22	5.4
0.6	42.6	7.2	3.5	0.26	0.27	11.3	3.4	1.7	0.24	0.20	5.5

Table 4 gives the collisional and FO loss fractions of alphas in the monotonic and hollow current equilibria with *I/B* = (2.5 MA)/(3.45 T) for the flat fusion source term $S = S_2$. From the data in these tables it follows that the main contribution to the neoclassical loss is from the toroidally trapped alphas ($L_{NC}{}^t$), while the radial diffusion loss of co- and counter-going particles, $L_{NC}{}^+$ and $L_{NC}{}^-$, respectively, are usually less than $(0.1 \div 0.3)L_{NC}{}^t$. The dependencies of the collisional loss contributions $L_{NC}{}^t$, $L_{NC}{}^+$ and $L_{NC}{}^-$ on the toroidal current hole size or on the total plasma current value I can be rather weak or even non-monotonic (similar to the total NC loss of alphas), but may also differ from each other. However, the total loss ($L_{FO} + L_{coll}$) increases monotonically with an enlargement of the current hole (position of x_m) as well as with a plasma current reduction.

Important from the point of view of the alpha loss effect on the first wall as well as on the plasma edge in a tokamak reactor is the problem of poloidal and pitch-angle distribution of the collisional loss of fusion alphas. Note that, in the case of an axisymmetric and quiescent plasma and an

axisymmetric poloidally smooth first wall, the half width of the poloidal distribution of the NC loss is determined by the typical pitch angle scattering induced change of the magnetic moment per bounce period, $\Delta\lambda \sim (\nu_\perp \xi^2 \tau_b)^{1/2} \sim 10^{-4}$-$10^{-3}$. The corresponding variation of the toroidal canonical momentum per bounce time, $\Delta P_\varphi^{\,\mathrm{coll}}$ [$\equiv(\partial P_\varphi/\partial\lambda)\Delta\lambda$], distributes the collisional loss of marginally confined orbits ($r_{max} \to a$) into a rather narrow range of poloidal angles

$$\Delta\theta^{coll} \cong \sqrt{\frac{2\left|\Delta P_\varphi^{\,coll}\right|}{\left|\partial^2 P_\varphi/\partial^2\theta\right|_{0.180}}} = \sqrt{\frac{2A\Delta\lambda}{1+\cos^2\zeta_a}} \qquad (5)$$

i.e. $\Delta\theta^{coll} \sim (1 \div 2)^\circ$. The effective half width of the loss distribution over the poloidal angle due to gyro motion, $\Delta\theta^{gyro}$, is even smaller ($\sim \rho_L/(qR) << 1^\circ$). The poloidal distributions of the collisional loss presented here are obtained supposing that they are formed by the drift of the guiding centre of lost particles due to the TF ripple perturbations of the toroidal canonical momentum ΔP_φ per bounce time. Following [19] it is supposed that $L(\theta)$ is shaped by randomly distributed ΔP_φ. Resulting ripple-induced orbit relocations per bounce period in the $\{R, Z\}$-plane distribute the neoclassical loss over the wall in the range of poloidal angles $0 \le \theta \le \theta_{\max}$ for co-moving particles and in the range $180^\circ - \theta_{max} \le \chi \le 180^\circ$ for counter- moving particles. Here χ_{max} is determined by the expression

$$\chi_{max} \cong \sqrt{\frac{2\Delta P_{\varphi\,max}}{\left|\partial^2 P_\varphi/\partial^2\theta\right|_{0,180}}} = 2\sqrt{\frac{\left|\cos\zeta_a\right|}{1+\cos^2\zeta_a}}\,A\Delta \qquad (6)$$

where Δ is the normalized maximum ripple perturbation of toroidal canonical momentum per bounce period. For circulating particles it is determined by the maximum ripple magnitude along the orbit, i.e.

$$\Delta = \Delta^c \approx \delta \quad \frac{1+\xi^2}{2} \quad \left.\frac{Y}{\langle Y\rangle}\right|_{\theta=0} \qquad (7)$$

where δ denotes the ripple magnitude and $Y/\langle Y\rangle = \mathrm{O}(1)$ is a factor of order unity accounting for FS non-circularity effects [15]. For well-trapped particles with banana turning points ($V_\parallel = 0$) far from the equator, Δ is determined by the resonant ripple induced vertical shift of banana tips [20]

$$\Delta = \Delta^t \approx \delta \left.\left(\frac{\pi N q R_a}{r\left|\sin\theta\right|} \quad \frac{Y}{\langle Y\rangle}\right)^{1/2}\right|_{\xi=0} \qquad (8)$$

For lost trapped alphas with banana tips near the JET equator where the ripple magnitude is extremely small, Δ is determined by Equation (7), i.e. by the P_φ-perturbation induced by the maximum ripple magnitude along the orbit. For low TF ripple magnitudes in JET ($\delta \le 0.001$–0.002) the maximum ripple induced poloidal shift of NC loss is $\chi_{max} \le (10$–$20)^\circ$ which, however, significantly exceeds the poloidal broadening of loss distribution due to pitch-angle scattering ($\Delta\chi^{coll}$) and due to gyration ($\Delta\chi^{gyro}$).

Figure 15 demonstrates the distribution of the calculated collisional (+FO) loss over the poloidal and pitch angles for *I/B* = (2.5 MA)/(3.45 T) hollow current equilibria with $x_m = 0.45$ and $x_m = 0.6$. It is seen that the neoclassical collisional loss of co- and counter-moving alphas are strongly localized in poloidal angle just below the mid-plane, and the cone loss is localized in pitch angle in the vicinity of pitch angles $\zeta = \zeta_s(E)$ of the lost fattest bananas. The maximum collisional fluxes result from the NC loss of trapped alphas at poloidal angles ~10˚ and pitch angles ~ 60˚, as well as from the cone loss of fattest bananas at pitch-angles ~ 50˚–70˚ (corresponding to the pitch angles of lost fattest bananas with energies 220 keV < E < 3.5 MeV) and poloidal angles ~ 60˚–100˚. Because of the strong poloidal localization of the collisional loss, the maximum NC flux of toroidally trapped alphas even exceeds the maximum FO loss flux as apparent from Figure 15 (in spite of the fact that the total number of neoclassical loss of trapped particles is small compared to the FO loss, $L_{NCt} \sim 0.1 L_{FO}$) and the maximum heat load of NC loss is comparable to the maximum FO heat load. Correspondingly, the maximum cone loss flux is commensurable with the maximum FO loss flux. We note that cone losses are hardly distinguishable from the FO losses since they occur in a pitch-angle range that is very close to the pitch angles of lost fattest 3.5 MeV alphas, where the maximum of the FO loss is observed. Cone loss is clearly visible only in the case of a large current hole, e.g. $x_m = 0.6$, as it is seen in Figure 15b.

Poloidal distributions of both the total classical alpha flux (= total FO loss flux + total NC flux + total cone loss flux), $\Gamma(\theta) = \int d\zeta \sin\zeta \int dE E^{1/2} \Gamma(\zeta, E, \theta)$, and the corresponding total alpha heat flux, $W(\theta) = \int d\zeta \sin\zeta \int dE E^{3/2} \Gamma(\zeta, E, \theta)$, where $\Gamma(\zeta, E, \theta)$ denotes the angle- and energy-dependent loss flux, are shown in Figure 16 for various current profiles and various total toroidal currents. Contrary to the distribution of FO loss, the total classical loss distribution is characterized by two additional maxima at poloidal angles ~5˚–10˚ below the mid-plane being in correspondence with the NC loss contributions of co- and counter-going alphas.

The important quantities from the point of view of edge plasma physics are the maximum charged fusion product flux, $\Gamma_{\alpha\, max}$, and the corresponding maximum heat flux, $W_{\alpha\, max}$. It is convenient to express both these values via the averaged neutron flux, Γ_n, and the neutron heat load W_n(=14MeV Γ_n), i.e.

$$\Gamma_{\alpha\, max} = \Gamma_n L p, \; W_{\alpha\, max} = 0.25 W_n L_E p_E \qquad (9)$$

where L is the fast particle loss fraction and p is the peaking factor (the ratio of maximum alpha loss flux, $\Gamma_{\alpha\, max}$, to the flux of lost alphas averaged over the first wall, $\langle\Gamma\rangle \equiv \Gamma_n L$), L_E and p_E denote the alpha energy loss fraction and, respectively, the peaking factor for the poloidal distribution of the alpha heat flux. Accounting for the total alpha particle loss (FO + NC + Cone), we list in Table 5 the calculated maximum alpha fluxes normalized to the corresponding neutron fluxes (=products of peaking factors and loss fractions) for monotonic and hollow current profiles for *I/B* = (2 MA, 2.5 MA)/3.45T.

Table 5: Maximum particle and heat fluxes of fusion alphas produced by FO and collisional losses for various current profiles and various total plasma currents in JET taking the fusion source term $S = S_1$, (shot #51976). Alpha particle and alpha heat fluxes are normalized to the DT neutron and DT neutron heat fluxes, respectively. Collisonal losses take into account lost alphas with energies $E > 0.0625E_0 = 220$ keV.

I	*α-particle flux/neutron flux*				*α-particle heat flux/neutron heat flux*			
[MA]/x_m	*FO*	*FO + Cone*	*FO + NC^{co}*	*FO + NC^{ctr}*	*FO*	*FO + Cone*	*FO + NC^{co}*	*FO + NC^{ctr}*
2.5/0	0.43	0.56	1.8	0.13	0.11	0.13	0.35	0.03
2.5/0.45	0.78	1.0	1.7	0.10	0.20	0.23	0.28	0.03
2.5/0.6	1.1	1.5	2.1	0.11	0.27	0.33	0.28	0.03

The next important feature of the collisional and also of the FO alpha loss is their strong anisotropy in longitudinal energy. As seen from Figure 15 the absolute majority of alpha loss occurs at pitch angles $50^o < \zeta < 80^o$, i.e. with $0.6 > \xi (= V_{||}/V) > 0.2$, and only a small fraction of counter-circulating particles (<1%) is lost with $\xi < 0$.

Finally in Figure 17 we illustrate, for various radial positions of the current maximum, the energy spectra of neoclassical, $L_{NC} = L_{NC}^{\ t} + L_{NC}^{\ +} + L_{NC}^{\ -}$, and cone collisional losses. The maximum collisional loss takes place at rather high energies ($E > 3$ MeV) because of the strong inhomogeneity of the initial distribution of confined 3.5 MeV alphas in radial and pitch-angle coordinates. Qualitatively different are the spectra of cone and NC losses. For NC loss effect of the current hole is important only at high ($E > 3$ MeV) and low ($E < 1$ MeV) energies. The decrease of NC loss at $E > 3$ MeV with the increase of the current hole size is due to the strong reduction of the number of confined 3.5 MeV alphas (which can potentially contribute to the NC loss). On the other hand, at low energies the enlargement of particle orbit widths is the reason for the enhancement of NC loss with increasing x_m. Contrary to the NC loss, the cone loss is essentially affected by the toroidal current shape, also in the moderate energy range 1 MeV $< E <$ 3 MeV (Figure 17b). A next difference between NC and cone loss is the pronounced sensitivity of the latter to the profile of the fusion source. These peculiarities of the cone loss spectra are obviously due to the increase of the loss cone size in phase space with the enlargement of the current hole area and because of the increase of the number of alpha particles contributing to this loss at the plasma periphery.

5. DISTRIBUTION FUNCTION OF CONFINED ALPHAS

We now present the result of 3D in Constants-of-Motion space Fokker-Planck calculations of the alpha particle distribution function in JET hollow current equilibria. One may expect an enlarged effect of pitch-angle scattering and slowing down on the initial distribution function $f(E = E_0)$ in the presence of a current hole. Figure 18 displays the alpha distribution in the radial coordinate and the normalized magnetic moment at high ($E = 3.5$ MeV), moderate ($E = 1$ MeV) and low ($E = 250$ keV) energies for hollow and monotonic toroidal currents. It is seen that the current hole affects mainly the radial distribution of confined alphas. Thus in the case of the current hole with $x_m = 0.45$, the radial dependence of $f(r_{max}, \lambda, E = E_0)$ becomes flatter near the inner part of the confinement domains

($r_{max} \sim r_{min}(\lambda = 0)$) and turns out to be even non-monotonic at lower energies (Figures 18 g, h, i, j, k, l) contrary to the distribution in the case of a monotonic toroidal current (Figures 8 a, b, c, d, e, f).

Non-monotonic current profiles effect significantly the radial profiles of the alpha particle density, n_α, as well as the electron and ion power deposition profiles, $P_{\alpha i}$ and $P_{\alpha e}$, in the real radial coordinate. The corresponding FS averaged profiles of n_α, $P_{\alpha i}$ and $P_{\alpha e}$ are shown in Figure 19 a, b. As evident, a current hole results in the reduction of these values and also in their flattening. The current hole effect on the alpha bootstrap current, j_α, appears to be surprisingly low. The reason for that is the strong effect of loss cone and FO loss on the j_α. The corresponding bootstrap contributions can increase with a current hole enlargement in spite of the decrease of the density of confined particles. Note that the total alpha driven current $j_{\alpha\, tot}$, including that of alphas and also the electron reversed current can be represented as

$$j_{\alpha\, tot} = j_\alpha \left(1 - \frac{Z_\alpha}{Z_{eff}} (1 - g) \right) \qquad (10)$$

where $g \sim (r/R)^{1/2}$ stands for the trapped electron correction to $j_{\alpha\, tot}$ [20].

Figure 20 displays the distribution of alpha particle density and bootstrap current in poloidal cross-section in I/B = 2.5 MA/3.45 T JET hollow current equilibrium with $x_m = 0.6$. It is seen that non-averaged alpha particle density and bootstrap current are shifted outward to the low field area and alpha driven current even change the sign in the inward high-B part of cross section. Distribution of electron and ion power deposition in the JET poloidal cross- section for hollow current profile with $x_m = 0.6$ is shown in Figure 21. It is seen that, similarly to n_α and j_α, the corresponding deposition are strongly modulated over the poloidal angle with maximum at the outward low-B part of cross-section.

SUMMARY

Our predictive alpha loss calculation demonstrates that hollow current profiles in JET result in a moderate increase of FO losses of alphas if the current hole region is small, i.e. if the radial position of maximum current is $r_m/a < 0.5$. For such cases with $I > 2$ MA the FO loss fraction is less than 30% and the alpha induced heat load is less than 30% of the neutron first wall load.

The presence of a current hole leads to an enhanced axisymmetric collisional loss of alphas in the energy range $0.0625 < E/E_0 < 1$, amounting to about (6–12)% loss fraction at $I > 2.5$ MA.

The distribution function of confined alphas is essentially affected by hollow current profiles at moderate toroidal currents $I < 3$ MA. Also the alpha particle density profiles as well as the electron and ion power deposition profiles are strongly influenced by non-monotonic current profiles.

It is important that the current hole effect is qualitatively equivalent to the reduction of the total plasma current, so that the confinement degradation associated with the current hole can be compensated by the enlargement of I.

We note, that TF ripple collisional transport [18] has not yet been taken into account here, however, it may play a substantial role even in the present low-ripple JET cases with hollow current profiles.

ACKNOWLEDGEMENTS

The authors are indebted to Yu. Baranov, A. Gondhalekar, W. Fundamenski, T. Hender, V.Kiptily, S. Kuhn, V. Parail, E. Solano, and D.Tskhakaja for fruitful discussions and constructive criticism and to N. Hawkes for supplying the data for Figure 2b.

This work has been partially carried out within the Association EURATOM-OEAW project P4 and under the European Fusion Development Agreement. The content of the publication is the sole responsibility of its authors and does not necessarily represent the views of the European Commission or its services.

REFERENCES

[1] C. Gormezano *et al.*, Phys. Rev. Lett. **80**, 5554 (1998).
[2] N.C. Hawkes *et al.*, Phys. Rev. Lett., **87**, 115001 (2001).
[3] T. Fujita *et al.*, Phys. Rev. Lett. **87**, 245001 (2001).
[4] H. Tamai *et al.*, Proc. 29th EPS Conf. Pl. Phys. & Contr. Fus., Montreux, June 2002.
[5] R.J. Bickerton, J.W. Connor, J.B. Taylor, J. Natl. Phys. Sci. **229**, 110 (1971).
[6] B.B. Kadomtsev, V.D.Shafranov, Proc. 4th IAEA Conf. Pl. Phys. & Contr. Nucl. Fus. Res., Madison, 1971, Vol II, p 479.
[7] Ya.I. Kolesnichenko, *et al.*, Proc. 9th IAEA Conf. Pl. Phys. & Contr. Nucl. Fus. Res., Baltimore, Sept. 1982, Vol III, p 349.
[8] C. Kessel *et al.*, Phys. Rev. Lett. **72**, 1212 (1994).
[9] F.M. Levington *et al.*, Phys. Rev. Lett. **75**, 4417 (1995).
[10] E.J. Strait *et al.*, Phys. Rev. Lett. **75**, 4421 (1995).
[11] C.D. Challis *et al.*, Plasma Phys. Contr. Fus. **43**, 861 (2001).
[12] V. Goloborod'ko *et al.*, Nucl. Fusion **35**, 1531 (1995).
[13] K. Schoepf *et al.*, Kerntechnik **67**, 285 (2002); and BCP.POS. 4 at Int. Symp. Fusion Nuclear Technology, San Diego, USA, April 2002.
[14] R. Ellis III *et al.*, APS Meeting, November, 2002.
[15] V.A. Yavorskij *et al.*, Plasma Phys. Contr. Fusion, **43**, 249 (2001).
[16] T.E. Stringer, Plasma Phys. **16**, 651(1974).
[17] V.P. Nagorny, V.A.Yavorskij. Proc. 15th EPS Conf. Pl. Phys. & Contr. Fus. & Plasma Heating, Dubrovnik, May 1998, Vol II, p 522.
[18] V.A. Yavorskij *et al.*, Nucl. Fusion **38**, 1565 (1998).
[19] V. Goloborod'ko, V.A. Yavorskij, Nucl. Fusion **29**, 1025 (1989).
[20] S.P. Hirshman, Phys. Fluids **31**, 3150 (1988).

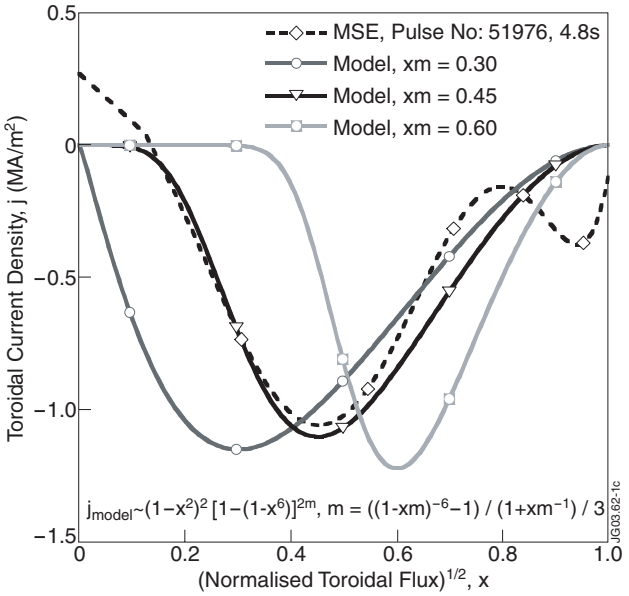

Figure 1: Model and reference MSE hollow current profiles in JET (Pulse No: 51976)

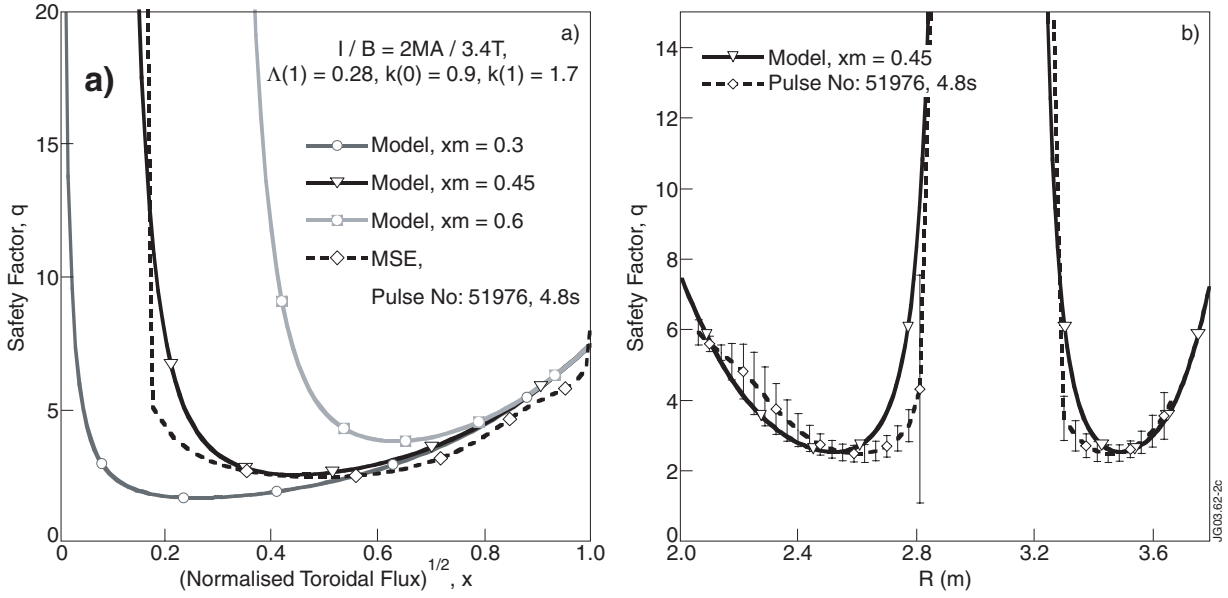

Figure 2: Safety factor profiles corresponding to hollow j *profiles of Figure 1*

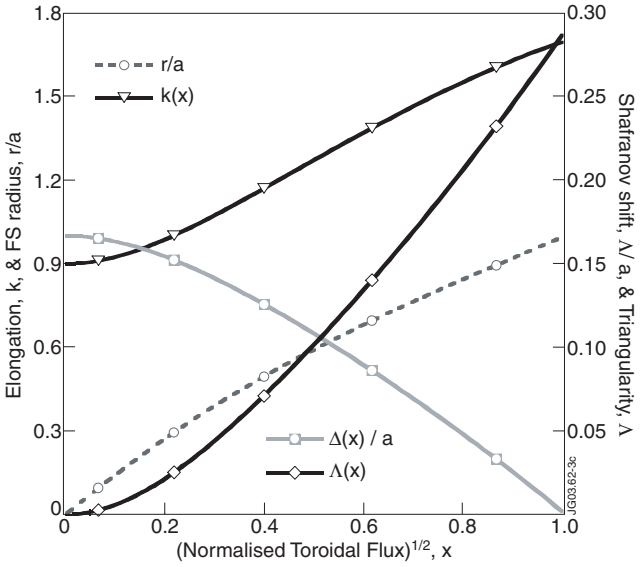

Figure 3: Profiles of reconstructed FS parameters

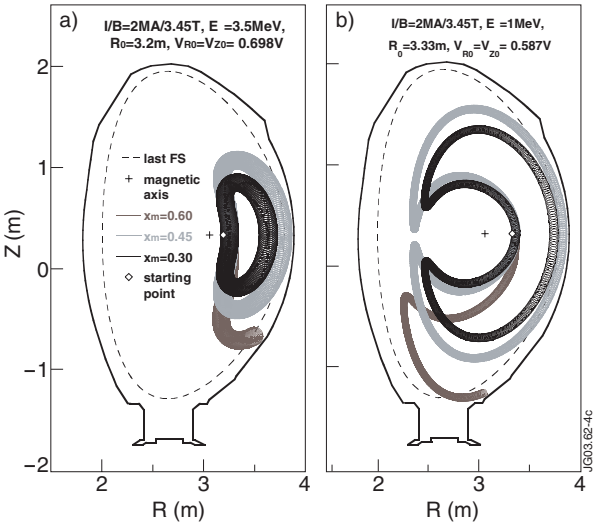

Figure 4: Gyro-orbits of 3.5MeV and 1MeV alphas for different hollow currents but identical initial conditions and same outmost flux surface

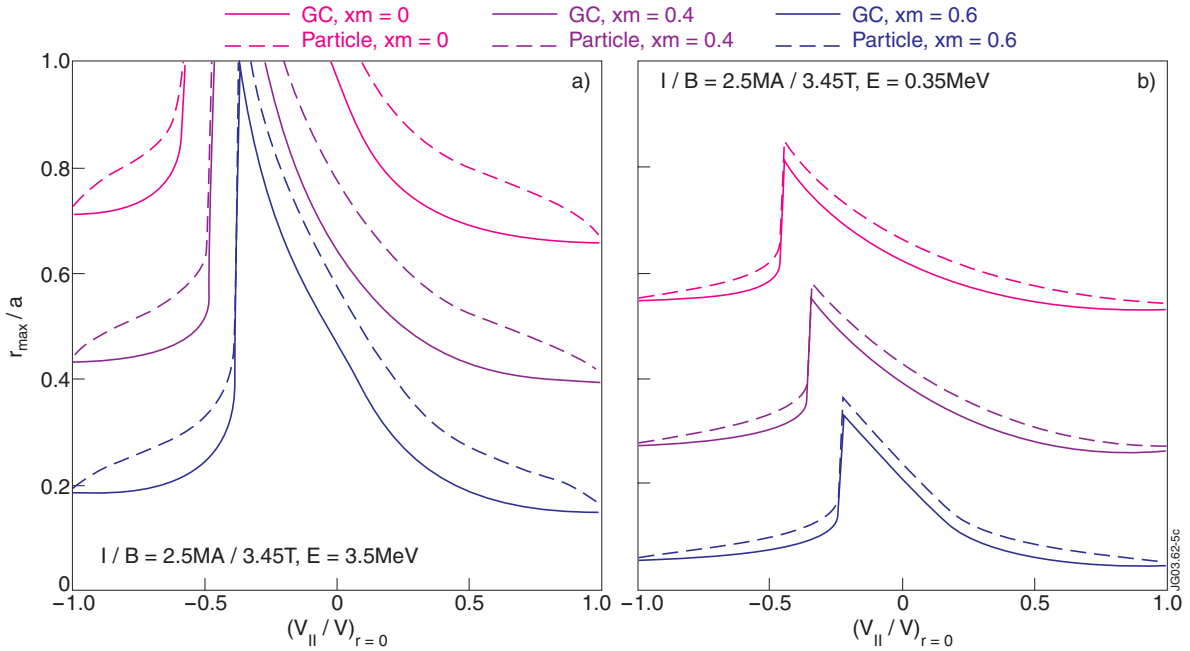

Figure 5: Maximum FS radius, r_{GCmax}, of the guiding centre along the drift orbits of 3.5MeV and 0.35MeV alphas passing through r = 0, as a function of the pitch angle cosine $\xi = V_{II}/V$ at r = 0, for monotonic and hollow current profiles in (2.5MA)/(3.45T) JET discharges. Dashed lines corresponds to the maximum radial coordinate of alpha particles demonstrating the finite gyro-radius effect

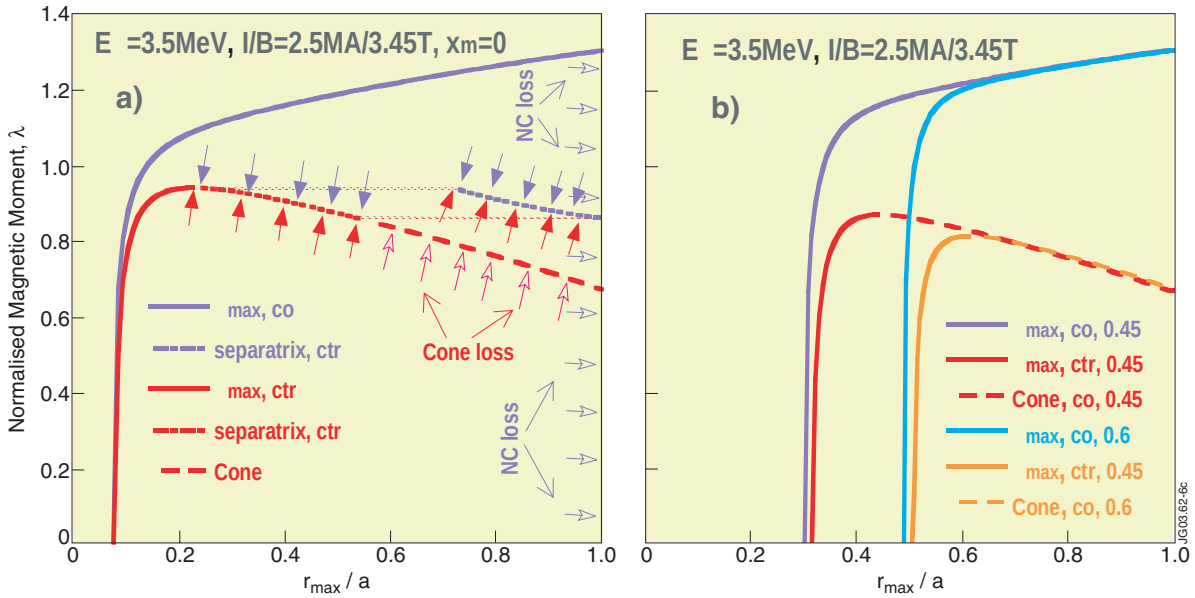

Figure 6: Confinement domains of 3.5MeV alphas in the λ- r_{max} plane for monotonic (X_m = 0) and hollow current profiles (X_m = 0.45, 0.6).

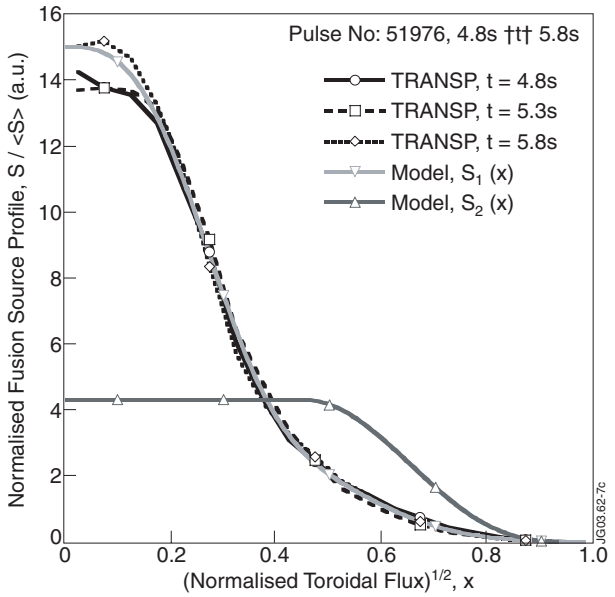

Figure 7: TRANSP fusion source profiles for shot #51976 for times 44.8s, 45.3s and 45.8s and model (Equation (4)) fusion source profiles normalized to their volume-averaged values, ⟨S⟩ ≡ ∫drS/∫dr

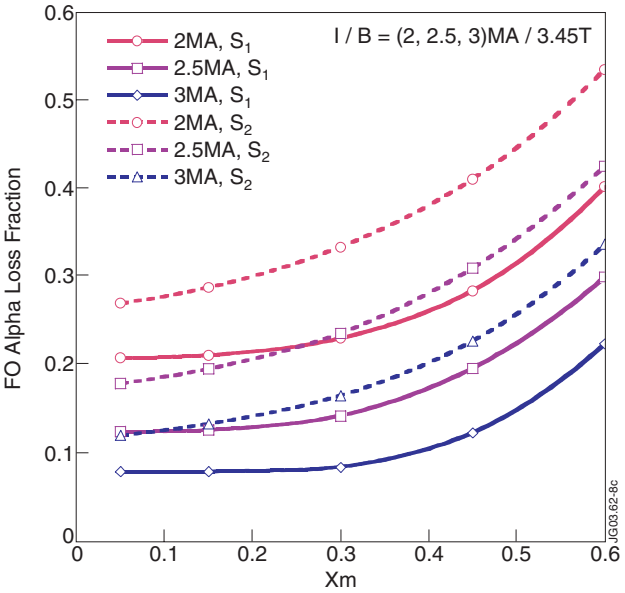

Figure 8: First orbit loss vs maximum current position for plasma currents 2 MA, 2.5 MA and 3 MA and different fusion source term profiles

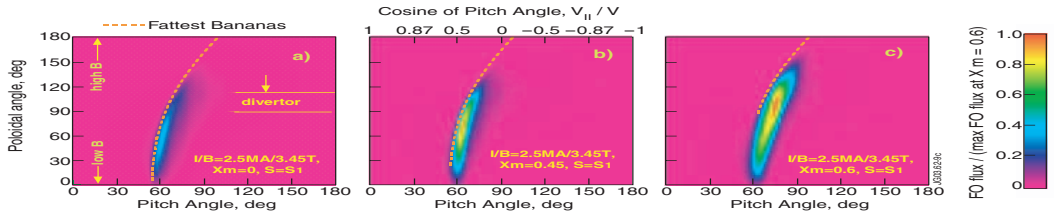

Figure 9: Distribution of FO alpha flux over the pitch angle ζ and the poloidal angle θ for monotonic and hollow current profiles at I/B *= (2.5MA)/(3.45T). The poloidal angle θ is determined as sin*θ *= -Z/2.9m and is counted clockwise from the point of minimum* B *at the mid-plane (R = 3.9m).*

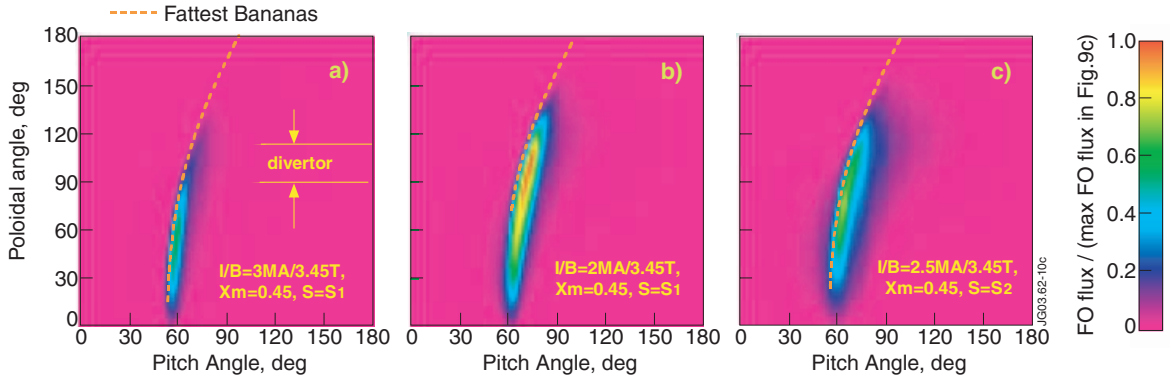

Figure 10: Distribution of FO alpha flux over the pitch and poloidal angles for a hollow current profile (x_m *= 0.45) at various total toroidal currents and fusion source profiles.*

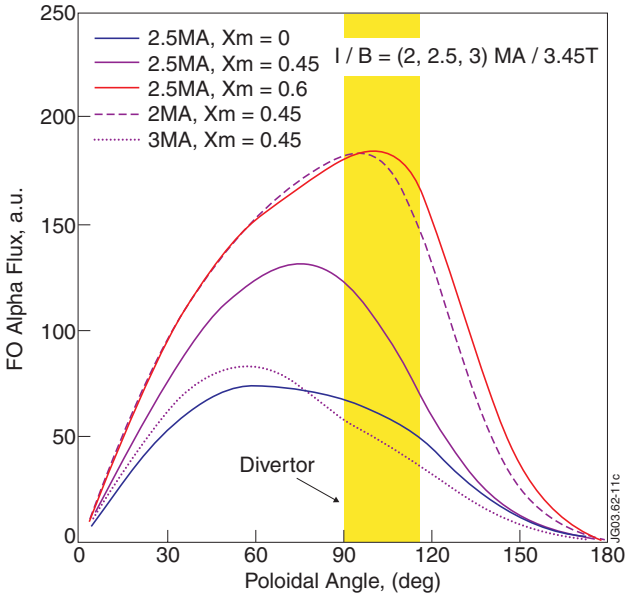

Figure 11: Distribution of the pitch-angle averaged FO alpha flux, $\Gamma(\theta) = \int d\zeta \Gamma(\zeta, \theta)/\int d\zeta$*, over the poloidal angle for various current profiles and various total toroidal currents.*

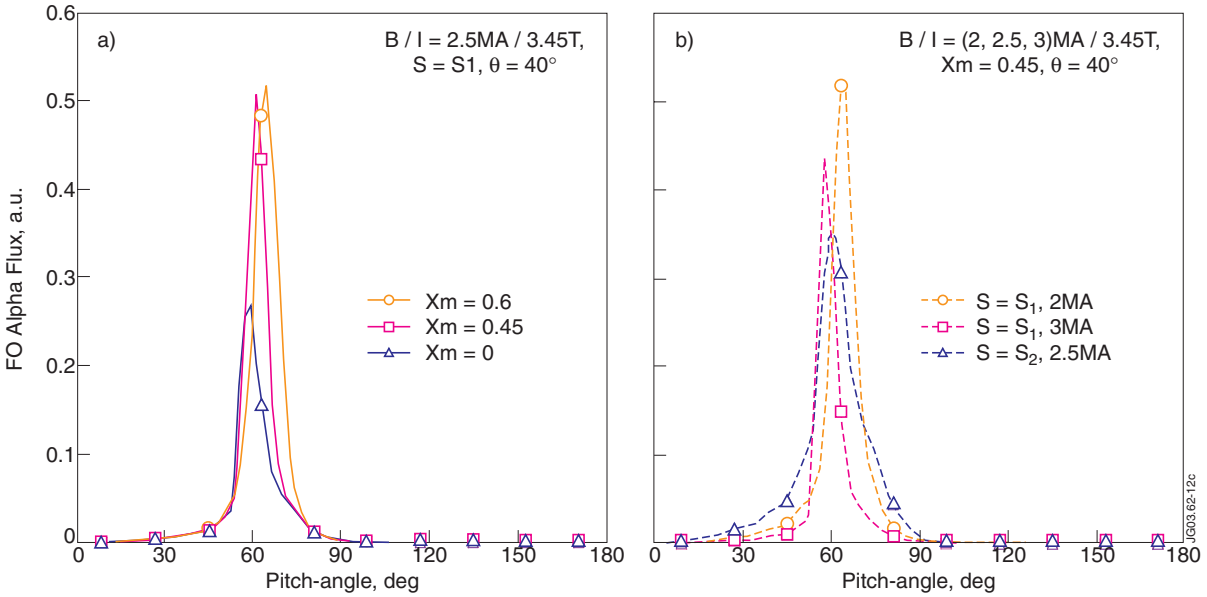

Figure 12: Distribution of FO alpha flux $\Gamma(\zeta, \theta)$ *over the pitch angle at* $\theta = 40^{\circ}$ *for various hollow current and fusion source profiles and for various total toroidal currents*

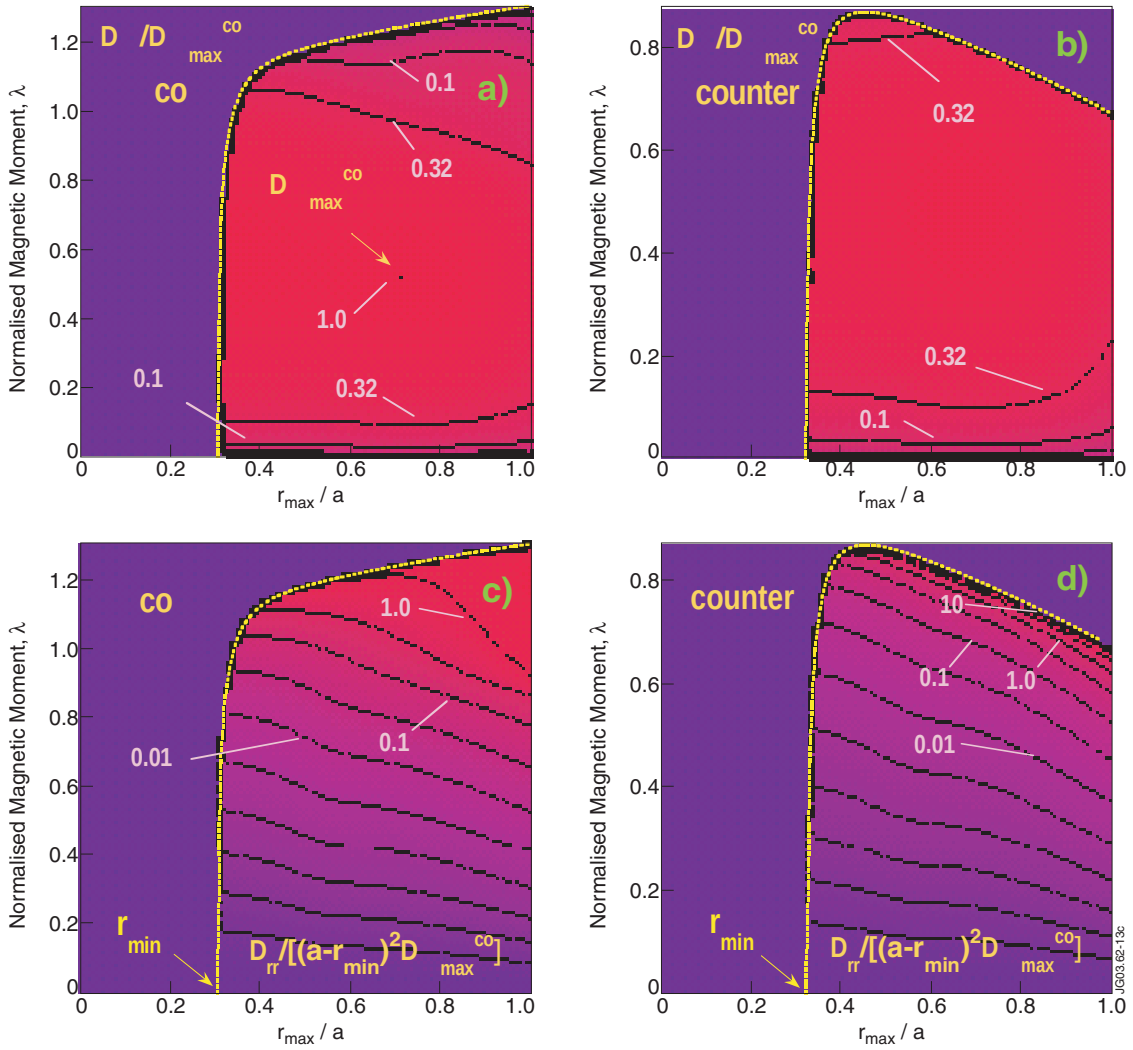

Figure 13: Contours of the bounce-averaged pitch-angle scattering diffusion coefficient, $D_{\lambda\lambda}$*, (Figures a and b) and contours of the bounce-averaged radial diffusion coefficient,* D_{rr}*, (Figures c and d) of 3.5 MeV co-going (Figures a, c) and counter-going (Figures b, d) alphas in the* $\{\lambda, r_{max}\}$*-plane in* I/B = 2.5MA/3.45T *JET hollow current equilibrium with* $x_m = 0.45$*.* $D_{\lambda\lambda}$ *is normalized to its maximum value (max*$\{D_{\lambda\lambda}\} = 0.02s^{-1}$*) that occurs for trapped particles with* $\lambda = 0.5$*,* $r_{max} = 0.7$a *and* D_{rr} *is normalized to the value* $[a - r_{min}(\lambda = 0, \sigma)]^2 \times max\{D_{\lambda\lambda}\}$

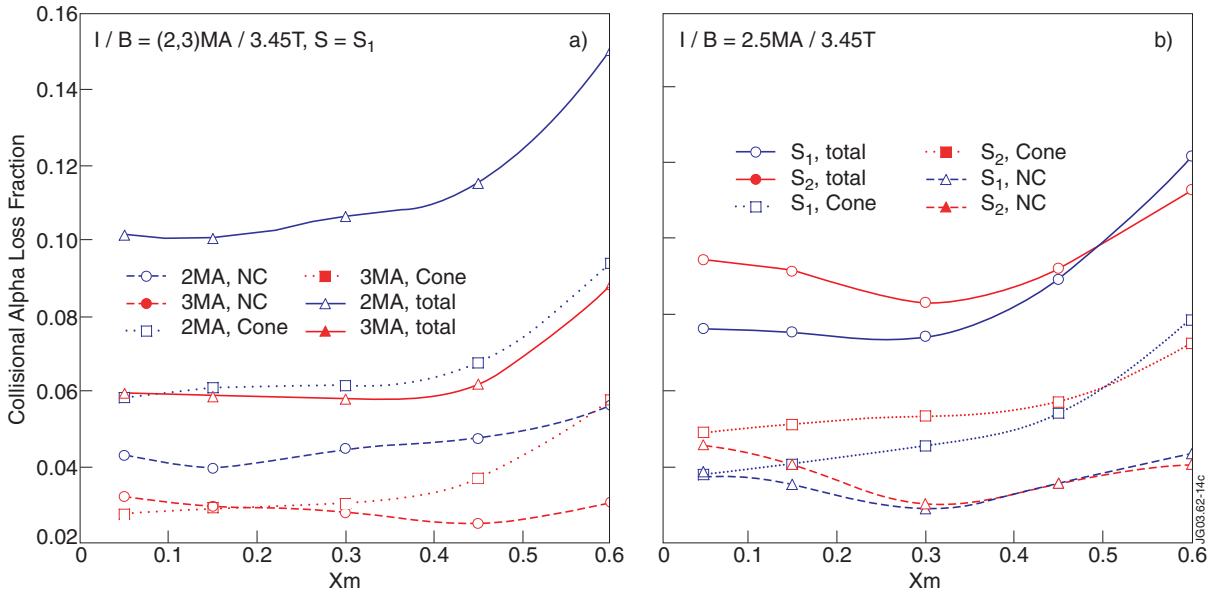

Figure 14: Collisional loss fractions L_{NC} *and* L_{cone} *of alphas in the energy range 0.0625< E/E*$_0$ *<1 caused by their radial neoclassical diffusion and scattering into the loss cone through the passing/trapped boundary, respectively, as well as the total collisional loss fraction* $L_{total} = L_{NC} + L_{cone}$ *as a function of the radial position of the hollow current maximum*

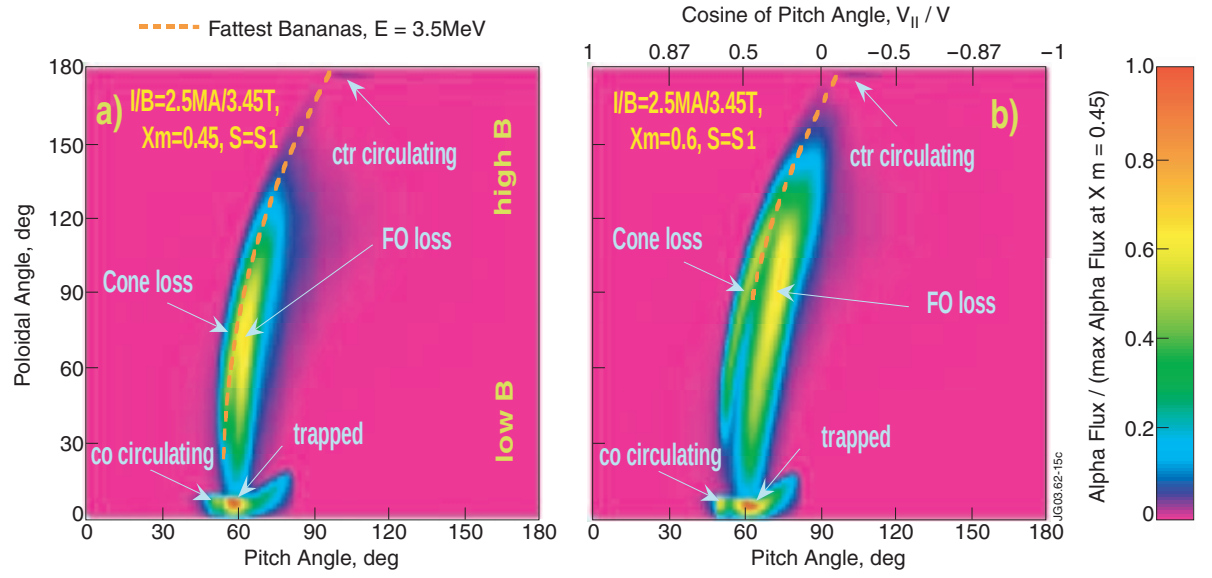

Figure 15: Distribution of collisional + FO alpha flux over the pitch and poloidal angles in I/B = *(2.5 MA)/(3.45 T) JET hollow current equilibrium for various hollow current profiles*

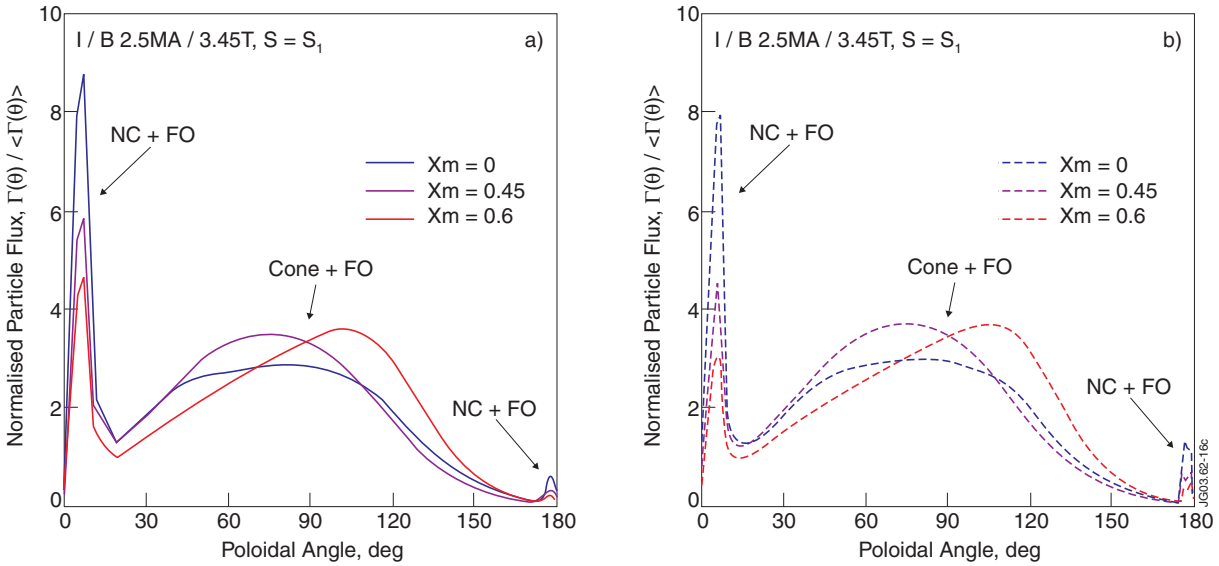

Figure 16: Poloidal distributions of the total classical alpha flux and total alpha heat flux, $\Gamma(\theta) = \int d\zeta \Gamma(\zeta, \theta) / \int d\zeta$, *over the poloidal angle for various current profiles and various total toroidal currents.*

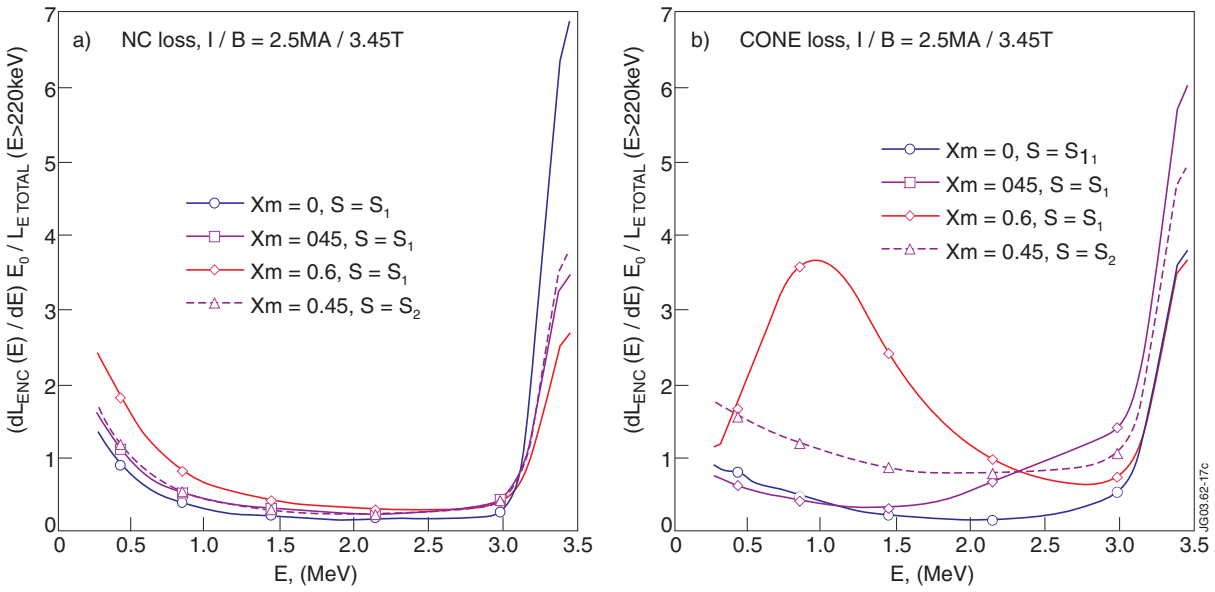

Figure 17: Energy spectra of collisional + FO alpha flux over the pitch and poloidal angles in I/B = *(2.5 MA)/(3.45 T) JET hollow current equilibrium for various hollow current profiles*

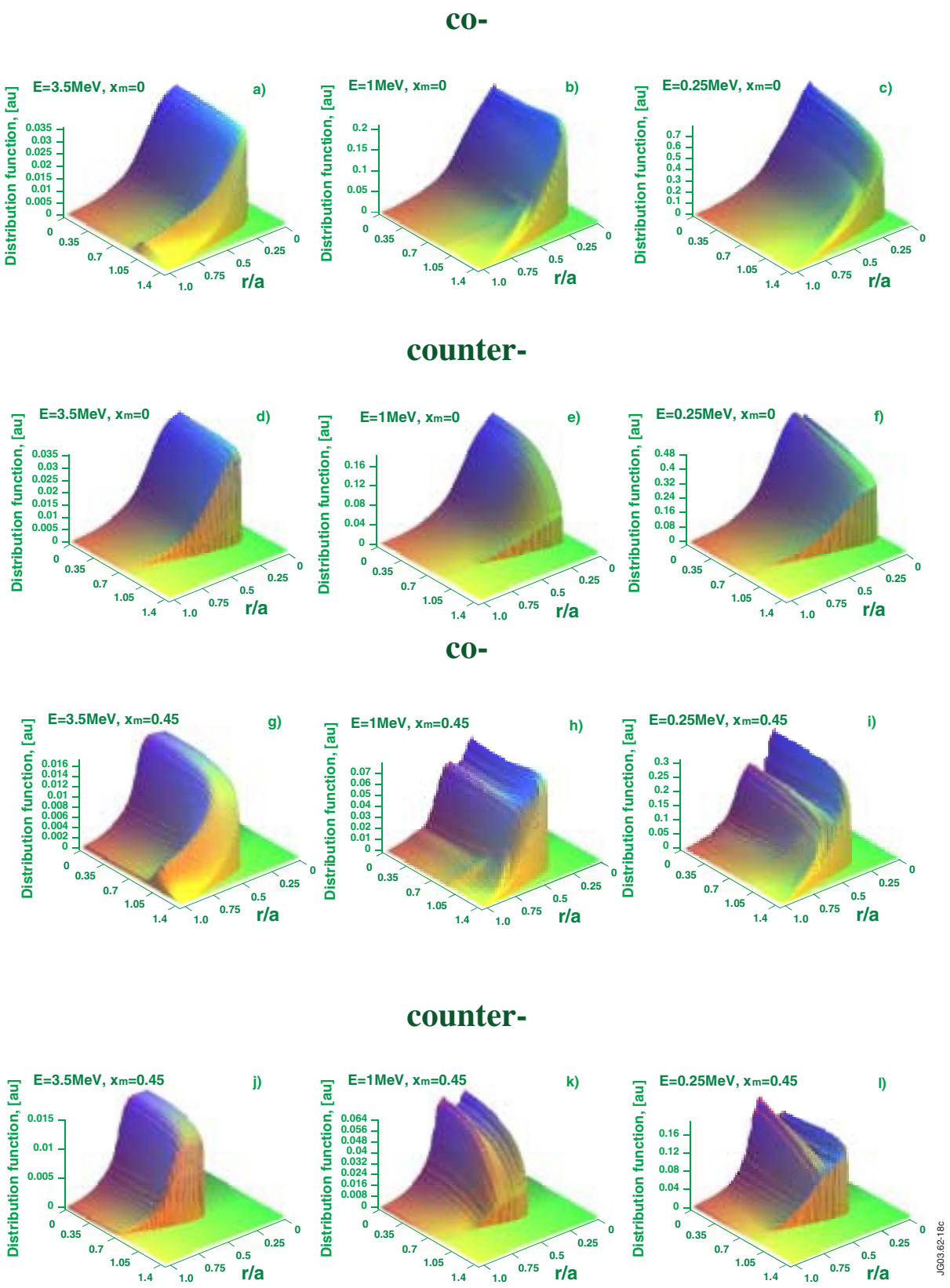

Figure 18: Effect of a non-monotonic current profile on the distribution function of confined alpha particles in JET at I/B=*(2.5 MA)/(3.45 T) and for the steep fusion source term,* $S = S_1$

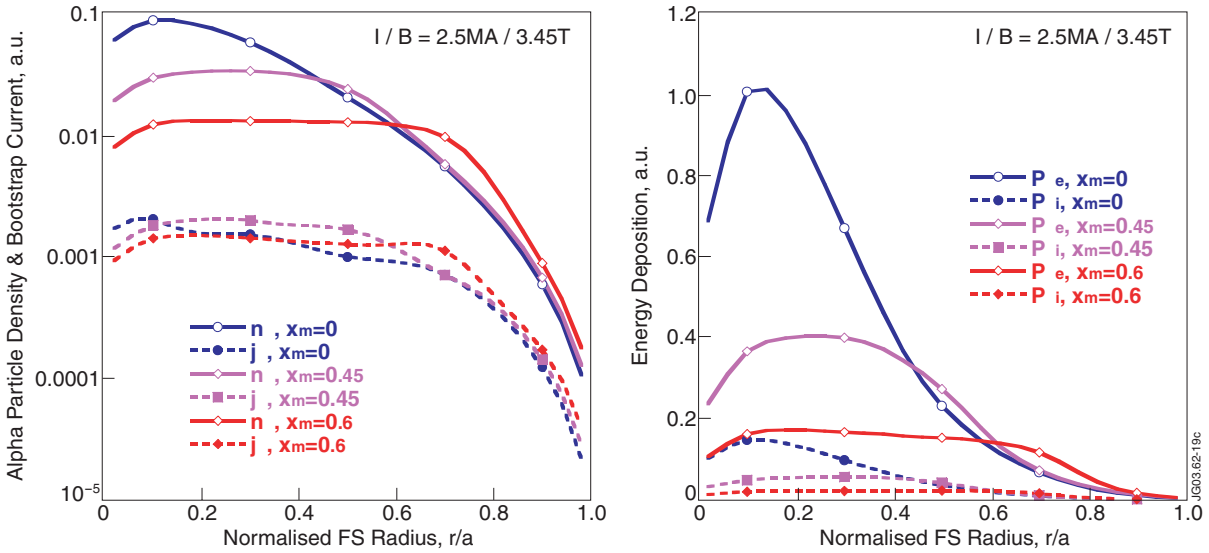

Figure 19: Profiles of alpha particle density, bootstrap current and electron and ion power depositions for various current profiles

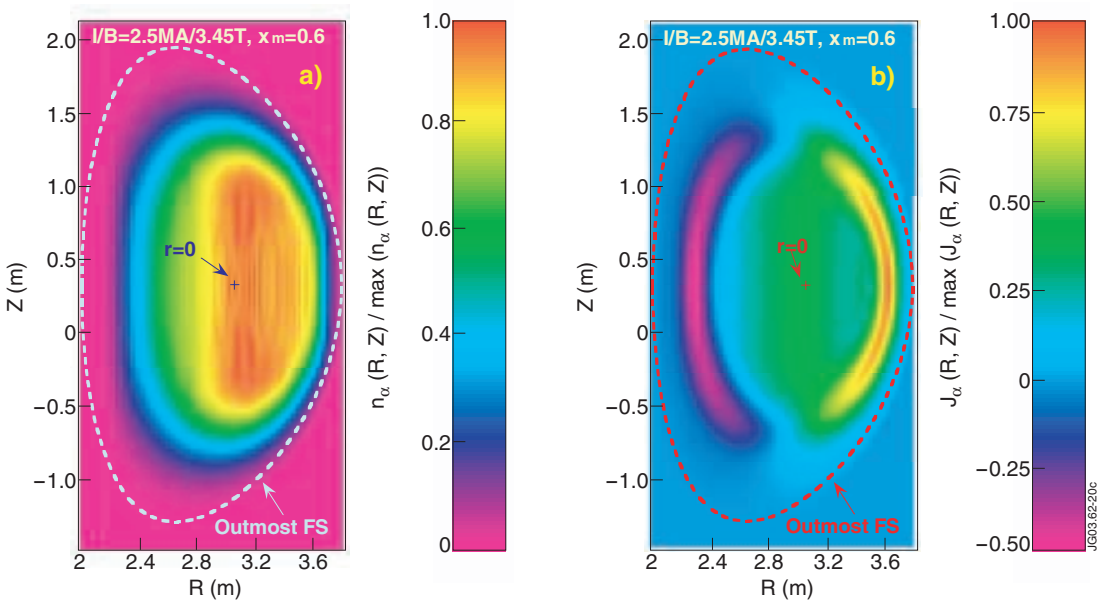

Figure 20: Distribution of alpha particle density and bootstrap current in the JET poloidal cross-section for hollow current profile with $x_m = 0.6$

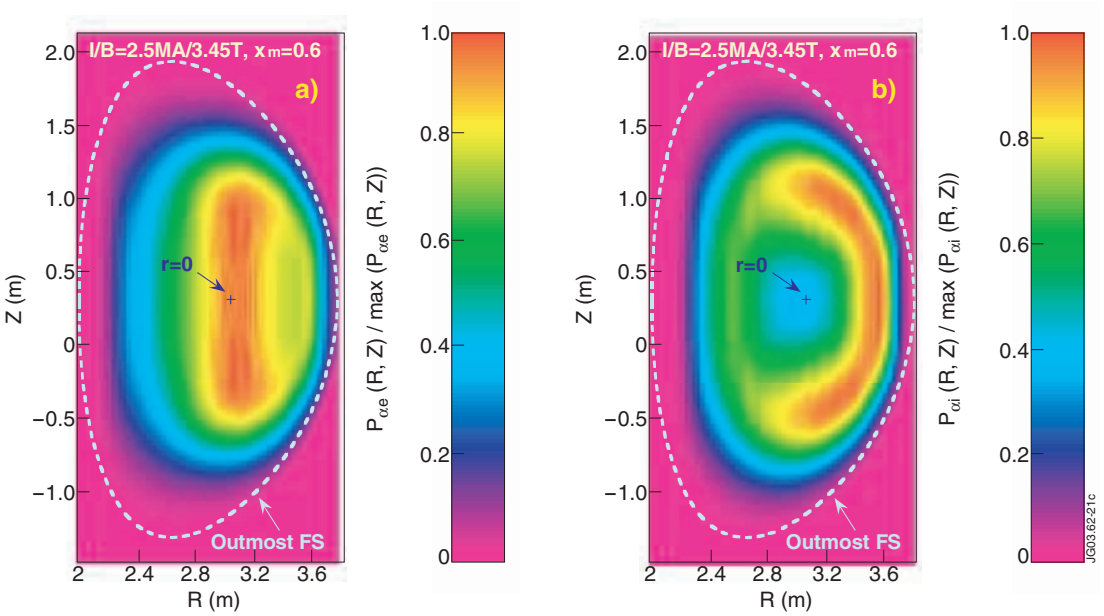

Figure 21: Distribution of electron and ion power depositions in the JET poloidal cross-section for hollow current profile with $x_m = 0.6$